MECHANICAL EQUILIBRIUM OF THICK, HOLLOW, LIQUID MEMBRANE CYLINDERS

RICHARD E. WAUGH AND ROBERT M. HOCHMUTH
Department of Biophysics, University of Rochester, School of Medicine and Dentistry, Rochester, New York 14642; and Department of Mechanical Engineering and Materials Science, Duke University, Durham, North Carolina 27706

ABSTRACT The mechanical equilibrium of bilayer membrane cylinders is analyzed. The analysis is motivated by the observation that mechanically formed membrane strands (tethers) can support significant axial loads and that the tether radius varies inversely with the axial force. Previously, thin shell theory has been used to analyze the tether formation process, but this approach is inadequate for describing and predicting the equilibrium state of the tether itself. In the present work the membrane is modeled as two adjacent, thick, anisotropic liquid shells. The analysis predicts an inverse relationship between axial force and tether radius, which is consistent with experimental observation. The area expansivity modulus and bending stiffness of the tether membrane are calculated using previously measured values of tether radii. These calculated values are consistent with values of membrane properties measured previously. Application of the analysis to precise measurements of the relationship between tether radius and axial force will provide a novel method for determining the mechanical properties of biomembrane.

INTRODUCTION

When a red cell that has adhered to a surface is subjected to a fluid shear force, long, thin hollow membrane cylinders or "tethers" are readily extracted from the body of the cell as shown in Fig. 1 *a* (Hochmuth et al., 1973). As long as the fluid shear force exceeds a value of $\sim 10^{-6}$ dyn, this tether will steadily increase in length because of the flow of membrane material from the cell body. A rapid increase in the force on the cell produces a rapid increase in the length of the tether without the addition of material from the cell. This, in turn, produces a decrease in the radius of the tether, which can be detected under the microscope as a lightening of the tether shadow. Thus, there is an inverse relation between tether force and tether radius.

As shown in Fig. 1 *b*, it is also possible to extract a tether from the spherical body of a red cell that has been aspirated into a pipette (Hochmuth et al., 1982). In this particular experiment, the radius of the tether (which is either invisible or appears as a faint shadow under the microscope) can be determined by using the condition that the membrane surface area is conserved (Hochmuth and Evans, 1982). Thus, the decrease in the surface area of the membrane material within the pipette is approximately balanced by an increase in the membrane surface area of the tether as it increases in length. The former is proportional to the pipette radius and the change in length of the membrane projection within the pipette, whereas the latter is proportional to the tether radius and the change in length of the tether. Because every quantity in this material balance is known except the tether radius, the value for the tether radius can be calculated readily. A typical value is 20 nm. Hochmuth et al. (1982) have observed that the radius varies inversely and reversibly with the tension in the membrane of the cell. Because the membrane tension times the circumference of the tether is equal to the tether force (Hochmuth and Evans, 1982; Waugh, 1982*a*), we again conclude that the radius is inversely related to the force on the tether.

In addition to tether formation from red cell membranes, tethers can be extracted from large phospholipid vesicles (Waugh, 1982*b*). These experiments show that tethers can be formed from a bilayer membrane that does not have an associated membrane skeleton, and that tethers formed from bilayer membranes with no shear rigidity can support significant axial loads under static conditions. This simple observation reveals the inadequacy of thin shell theory to describe the mechanical equilibrium within the tether. In a thin membrane with no shear rigidity, the stress resultants must be isotropic under static conditions (Waugh, 1982*a*). However, as we will show, the circumferential stress resultant in the tether is much smaller than the axial stress resultant. Thus, under the loading conditions in tether formation experiments, the equations of equilibrium for a thin shell are not satisfied for a membrane with isotropic stress resultants.

The experimental observations discussed above indicate that there is an inverse relation between the tether radius and the force on the tether and that this relationship exists

Address correspondence to Dr. Richard E. Waugh, Box BPHYS, University of Rochester Medical Center, 601 Elmwood Avenue, Rochester, NY 14642.

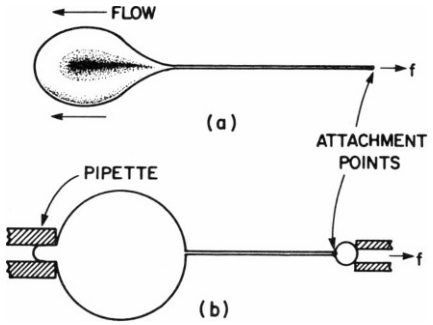

FIGURE 1 Schematic illustration of tether formation experiments. (*a*) In the flow channel, point-adherent cells are subjected to fluid shear stress generated by flow in the channel. When the force on the cell exceeds 1.0×10^{-6} dyn, a tether forms between the body of the cell and the attachment site. (*b*) Hypotonically swollen cells are aspirated into a glass micropipette. The cell adheres to a glass bead that is withdrawn by a second pipette at a fixed rate. The tether radius can be determined from measurements of the tether length, the pipette radius, and the displacement of the cell projection in the pipette as the tether forms. The membrane force resultant (tension) can be determined from the applied suction pressure and the cellular dimensions.

in the absence of significant membrane shear rigidity. Thus, the goal of the analysis presented here is to obtain an inverse force–radius relationship in terms of the "elasticity" of the membrane material in the tether and cell body. Our analysis, which is based on the mechanical equilibrium of thick, anisotropic liquid shells, shows how isotropic stresses in the plane of the membrane can produce highly anisotropic stress resultants. We assume that the tether membrane does not possess a shear rigidity because tethers can be formed from phospholipid vesicles. Furthermore, it is likely that tethers formed from red cell membrane have properties similar to tethers formed from phospholipid vesicles because red cell tethers appear to be devoid of cytoskeleton. Berk and Hochmuch (1986) have shown that the lateral mobility of fluorescent markers in the tether membrane is similar to the mobility of probes in spectrin-free erythrocytes (Koppel et al., 1981). Also, preliminary electron microscopic examination of tethers in thin section in our laboratory indicates a lack of spectrin within the tether.

A THICK ANISOTROPIC LIQUID SHELL

On a molecular scale the membrane consists of long, flexible, hydrocarbon chains joined to polar phosphate head groups. Observations of the mechanical behavior of lipid bilayer membranes above the phase transition indicate that the membrane is liquid-like, i.e., it has no surface shear rigidity to resist anisotropic stress in the plane of the surface. However, because the molecules are constrained by the hydrophobic effect to remain in the surface, there is a preferred thickness and area per molecule for the membrane, i.e., the membrane exhibits solid character in its resistance to change in thickness or surface area. Thus, the membrane is anisotropic in three dimensions but isotropic and fluid-like in the two dimensions of the surface plane.

Consider a curved element within the cylindrical tether membrane as shown in Fig. 2. The radial coordinate is r, the coordinate along the axis of the tether is z, and the angle of the rotation around z is ϕ. On the exposed surfaces of this membrane element we define the state of membrane stress with the principal stresses σ_z, σ_ϕ, and σ_r. The dimensions of the deformed element are related to its undeformed dimensions by the principal extension ratios:

$$dz = \lambda_z dz_o \tag{1}$$

$$dr = \lambda_r dr_o \tag{2}$$

$$r d\phi = \lambda_\phi r_o d\phi_o. \tag{3}$$

The constitutive relation for the shell must preserve the essential features of the membrane behavior, namely, small area expansivity and low (zero) shear rigidity. We make the further assumption that the membrane is volumetrically incompressible. (Jusitification for these assumptions is given in the Discussion.) We define the surface isotropic stress:

$$\bar{\sigma} = (\sigma_z + \sigma_\phi)/2, \tag{4}$$

and the surface shear stress:

$$\sigma_s = (\sigma_z - \sigma_\phi)/2. \tag{5}$$

The condition of zero surface shear rigidity requires that $\sigma_s = 0$. Therefore

$$\sigma_z = \sigma_\phi = \bar{\sigma}. \tag{6}$$

Because the resistance of the membrane to area changes is large (area strains are small), a simple linear relationship between the internal stresses and the fractional area change of the element, α, is sufficient to describe the material behavior:

$$\bar{\sigma} - \sigma_r = K\alpha(r), \tag{7}$$

where the radial dependence of α is indicated. Justification for the form of Eq. 7 is given in the Appendix. The elastic modulus K has units of dyn/cm^2. For the sake of simplicity we assume that K is independent of position within the shell. Clearly, in light of the inhomogeneity of the molecular structure in the radial direction this may be an oversimplification of the actual material behavior. However, our present goal is not to provide a detailed description of molecular interactions within the bilayer, but to model

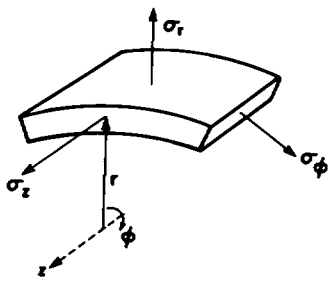

FIGURE 2 A material element within the membrane cylinder. The coordinate system and principal stresses of the membrane cylinder are shown. The radial coordinate is r, the axial coordinate is z, and the circumferential coordinate is ϕ. The principal stresses in these directions are σ_r, σ_z, and σ_ϕ, respectively.

with a minimum of complexity the essential features of the membrane behavior at high curvature.

With Eq. 7, the radial dependence of the difference between the surface-isotropic stress $\bar{\sigma}$ and the radial stress σ_r can be obtained by specifying the radial dependence of the fractional area change $\alpha(r)$. In terms of the principal extension ratios the fractional area change is given by

$$\alpha = \lambda_z \lambda_\phi - 1. \tag{8}$$

In terms of the area of the material element $A(r)$ it can be written:

$$\alpha(r) = \frac{A(r)}{A_o} - 1. \tag{9}$$

The unstressed area A_o is not a function of r because it is assumed that the stress-free state is a flat membrane. (Formally we take the stress-free cylindrical radius to be very large.)

For convenience, the area change $\alpha(r)$ can be expressed relative to the area change of the mid-surface $\alpha_{av} = A_{av}/A_o - 1$:

$$\alpha = \alpha_{av} + (\alpha - \alpha_{av}). \tag{10}$$

With the use of Eq. 9, the quantity $\alpha - \alpha_{av}$ can be written as

$$\alpha - \alpha_{av} = (1 + \alpha_{av})\,[A(r)/A_{av} - 1]. \tag{11}$$

The ratio of the area $A(r)$ to the area of the mid-surface A_{av} in terms of r is

$$\frac{A(r)}{A_{av}} = \frac{2\pi r L}{2\pi R_{av} L} = \frac{r}{R_{av}}, \tag{12}$$

where L is an arbitrary cylinder length and R_{av} is the radius of the mid-surface. The substitution of Eq. 12 into Eq. 11 and the substitution of this result into the right hand side of Eq. 10 gives

$$\alpha = \alpha_{av} + (1 + \alpha_{av})\left(\frac{r}{R_{av}} - 1\right). \tag{13}$$

Finally, when Eq. 13 is substituted into Eq. 7, we obtain an expression for the radial dependence of the stress difference

$$\bar{\sigma} - \sigma_r = K\alpha_{av} + K(1 + \alpha_{av})\left(\frac{r}{R_{av}} - 1\right). \tag{14}$$

Radial Force Balance

Because $\sigma_s = 0$, the axial and circumferential stresses are equal to the surface-isotropic stress (Eq. 6). For this case, a radial force balance on the material element shown in Fig. 2 gives

$$\frac{d\sigma_r}{dr} = \frac{\bar{\sigma} - \sigma_r}{r}. \tag{15}$$

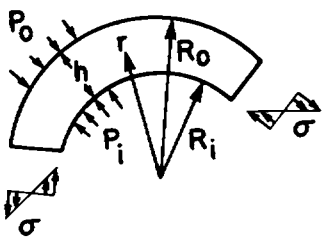

FIGURE 3 Schematic showing the quantities used in the radial force balance for a single thick shell. The circumferential stress is σ and the inner and outer pressures are P_i and P_o, respectively. The radial coordinate is r, the inner and outer membrane radii are R_i and R_o, and the membrane thickness is h.

When Eq. 14 is used to express the stress difference in terms of r, Eq. 15 can be integrated to obtain the radial dependence of σ_r (see Fig. 3). Application of the boundary condition, $\sigma_r = -P_i$ at $r = R_i$, and integration to an arbitrary r gives

$$\sigma_r(r) = -P_i + K\left[\frac{\alpha_i + 1}{R_i}(r - R_i) - \ln\left(\frac{r}{R_i}\right)\right]. \tag{16}$$

Application of a second boundary condition ($\sigma_r = -P_o$ at $r = R_o$) to Eq. 16 yields a relationship between the pressure difference $P_i - P_o$ and the tether dimensions and properties:

$$P_i - P_o = K\left[\frac{\alpha_{av} + 1}{R_{av}} h - \ln\left(\frac{R_o}{R_i}\right)\right], \tag{17}$$

where $h = R_o - R_i$, $R_{av} = (R_o + R_i)/2$, $\alpha_{av} = \alpha(R_{av})$ and the identity, $(\alpha_i + 1)/R_i = (\alpha_{av} + 1)/R_{av}$, has been used (see Eq. 12). The membrane equation of equilibrium for a cylinder can be recovered from Eq. 17 if we use a series expansion for the logarithmic term:

$$\ln(1 + x) = x - \frac{x^2}{2} + \frac{x^3}{3} - \frac{x^4}{4} + \cdots, \qquad -1 < x < 1. \tag{18}$$

After algebraic manipulation, we find:

$$\Delta P\, R_{av} = K_m \alpha_{av} - \frac{K_m}{12}\left(\frac{h}{R_{av}}\right)^2 + 0\left(\frac{h}{R_{av}}\right)^4 \cdots, \tag{19}$$

where $K_m = Kh$ is the membrane area expansivity modulus. The first term on the right hand side is the result for a thin membrane, and the second term gives the "first order" correction as the cylinder radius becomes small. The terms of order $(h/R_{av})^4$ are <1.0% of the first order correction, and these terms can be neglected without significant error.

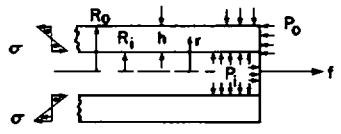

FIGURE 4 Schematic of the axial force balance for a single thick shell. The axial stress is σ, the inner and outer pressures are P_i and P_o, and the axial force is f. The radial coordinate is r, the inner and outer radii are R_i and R_o, and the membrane thickness is h.

Axial Force Balance

The summation of forces in the axial direction (Fig. 4) gives

$$\int_{R_i}^{R_o} \bar{\sigma}\, 2\pi r\, dr = P_i \pi R_i^2 - P_0 \pi R_0^2 + f, \tag{20}$$

where f is the axial force on the tether and $\sigma_z = \bar{\sigma}$. With Eqs. 14 and 16, Eq. 20 can be integrated to obtain:

$$\frac{f}{\pi R_{av}} = K_m \alpha_{av}\left(1 + \frac{h^2}{12R_{av}^2}\right) + \frac{K_m h^2}{12R_{av}^2}. \tag{21}$$

Here, as before, $K_m = K \cdot h$ and $R_{av} = (R_i + R_o)/2$. Note that $h^2/12R_{av}^2 \sim 0.01$ and can be neglected compared to one. Eqs. 19 and 21 can be combined to eliminate the term $K_m h^2/12R_{av}^2$ and recover the axial force balance for a thin membrane:

$$f + \Delta P(\pi R_{av}^2) = K_m \alpha_{av}(2\pi R_{av}). \tag{22}$$

Alternatively, Eqs. 19 and 21 can be combined to eliminate $K\alpha_{av}$ and obtain a relationship between the external forces and the tether radius:

$$\frac{f}{\pi} - \Delta P R_{av}^2 = \frac{K_m h^2}{6R_{av}}. \tag{23}$$

For tethers extracted from flaccid cells, the pressure difference, ΔP, is zero, and an inverse relationship between force and tether radius is readily obtained. For a tether extracted from a cell that has been aspirated into a pipette, typical values for ΔP and R_{av} are 3×10^3 dyn/cm^2 and 15.0 nm (Hochmuth et al., 1982). Thus, $\Delta P R_{av}^2 \simeq 0.75 \times 10^{-8}$ dyn, which is two orders of magnitude smaller than the force needed to form a tether ($\sim 1.0 \times 10^{-6}$ dyn) (Hochmuth et al., 1976). Thus, the pressure term in Eq. 23 can be neglected, and a simple inverse relationship between force and tether radius is obtained:

$$f \simeq \frac{\pi K_m h^2}{6} \cdot \frac{1}{R_{av}}. \tag{24}$$

Stress Resultants

Although the local state of internal stress is isotropic in the plane of the membrane, the stress resultants T_ϕ and T_z are not. The stress resultants are defined such that the product of the stress resultant times the length over which it acts is equal to the integral of the stress over the cross-section (see Fig. 5). In the z direction,

$$(2\pi R_{av})T_z = \int_{R_i}^{R_o} \bar{\sigma}\,(2\pi r)\, dr. \tag{25}$$

The integral is evaluated using Eqs. 14 and 16, and Eq. 21 is used to simplify the result:

$$T_z = \frac{f}{2\pi R_{av}} + \frac{P_i - P_o}{2} R_{av}\left[1 + \left(\frac{h}{2R_{av}}\right)^2\right] - h\frac{(P_i + P_o)}{2}. \tag{26}$$

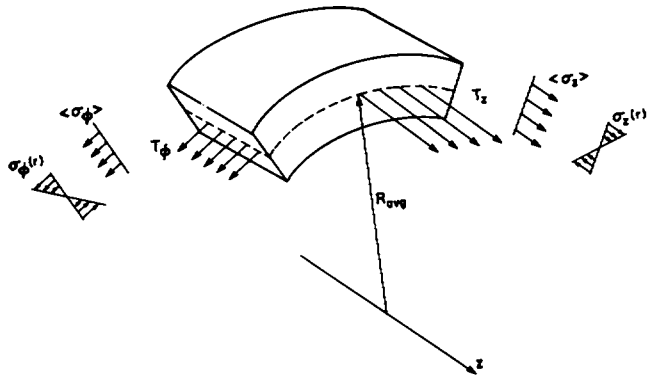

FIGURE 5 Cut-away view showing the stress resultants, T_ϕ and T_z, and the distribution of stress in the axial and circumferential directions. The total stress σ is shown as the sum of the mean stresses $\langle\sigma_z\rangle$ and $\langle\sigma_\phi\rangle$ and radially dependent stresses $\sigma_z(r)$ and $\sigma_\phi(r)$ for each direction. The stress resultants T_ϕ and T_z act at the midsurface, R_{av}.

In the ϕ direction, the stress resultant is defined by

$$T_\phi \cdot L = \int_{R_i}^{R_o} \bar{\sigma} \cdot L\, dr, \tag{27}$$

where L is an arbitrary length in the z direction (see Fig. 5). Again, using Eqs. 14 and 16 we evaluate the integral

$$T_\phi = (P_i - P_o)R_{av} - h\frac{(P_i + P_o)}{2}. \tag{28}$$

Note that these expressions for the stress resultants contain terms arising from the hydrostatic pressure. In the limit as the thickness of the membrane goes to zero, these terms also go to zero. Furthermore, it should be recognized that membrane tensions are measured experimentally relative to an "unstressed" state in which the hydrostatic pressure is non-zero. In the unstressed state, $f = 0$, $P_i = P_o = P_{atm}$, and the "reference" values for the stress resultants are: $T_{z_o} = T_{\phi_o} = -P_{atm}\, h$. Thus, the quantity $(-P_{atm}\, h)$ should be subtracted from Eqs. 26 and 28 to obtain expressions for experimentally measured stress resultants. Because the pressures applied to the cell are typically small compared with atmospheric pressure, and (as discussed above) the pressure term in Eq. 26 is small compared with the force,

$$T_z - T_{z_o} \simeq \frac{f}{2\pi R_{av}} \tag{29}$$

$$T_\phi - T_{\phi_o} \simeq (P_i - P_o)R_{av} - \frac{P_i - P_{atm}}{2} \cdot h - \frac{P_o - P_{atm}}{2} \cdot h. \tag{30}$$

It is important to recognize that although the stress

resultants approach the membrane limit as the shell becomes thin, the difference between the stress resultants in the thick shell can be appreciable, even though the stresses themselves are isotropic in the surface plane. To obtain the difference in terms of the membrane properties, we use Eqs. 19 and 21 to substitute for the force and pressure difference terms in Eqs. 26 and 28, and then take the difference of the results to obtain

$$T_z - T_\phi \simeq \frac{K_m h^2}{12 R_{av}^2}, \tag{31}$$

where terms of order $(h/R_{av})^4$ have been neglected.

TWO LIQUID SHELLS

A more general model than that presented in the previous section is one that consists of two uncoupled, thick liquid shells as shown in Fig. 6. Each shell represents a single lipid monolayer and together they form a bilayer. A two-dimensionally isotropic state of stress ($\sigma_\phi = \sigma_z$) exists in each shell. Between the shells we allow for the existence of a three-dimensionally isotropic state of stress given by the intramembrane pressure P_m. We postulate that along the hydrocarbon chains of the monolayers there are only two degrees of freedom for the transfer of momentum while at the end of the hydrocarbon chains at the terminal methyl groups there are three degrees of freedom and thus, in this region momentum can be transferred in three directions to create an isotropic pressure P_m.

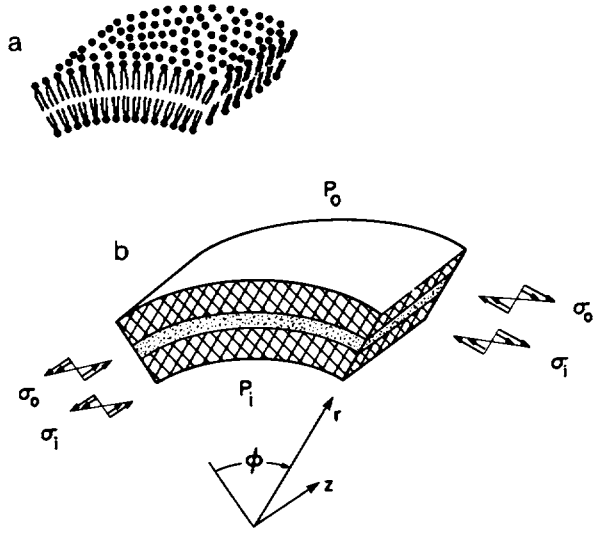

FIGURE 6 The double thick-shell model. (*a*) Schematic of lipid bilayer showing the lamellar structure. There is a "slip plane" between the two monolayers that allows the two layers to deform independently in the surface plane. (*b*) Schematic of the continuum model is used to approximate the bilayer. The radially dependent stresses are depicted for the inner (σ_i) and outer (σ_o) layers. The slip plane is depicted as a thin region of isotropic fluid. The cylindrical coordinates, r, ϕ, and z, and the inner and outer pressures, P_i and P_o, are shown.

Radial Force Balance

Fig. 7 gives a cross-sectional view of two liquid shells. To simplify the analysis, each shell has the same thickness h'. The distance between the shells is h_m and the intramembrane pressure is P_m.

The radial dependence of σ_r in the inner and outer shells is obtained analogously to the derivation of Eq. 16. We integrate over the inner shell from the inner boundary, $\sigma_{r_i} = -P_i$ at $r = R_i$, and we integrate over the outer shell from the outer boundary, $\sigma_{r_o} = -P_o$ at $r = R_o$:

$$\sigma_{r_i} = -P_i + K_i\left[\frac{\alpha_{av_i} + 1}{R_{av_i}}(r - R_i) - \ln\left(\frac{r}{R_i}\right)\right] \tag{32}$$

$$\sigma_{r_o} = -P_o - K_o\left[\frac{\alpha_{av_o} + 1}{R_{av_o}}(R_o - r) + \ln\left(\frac{r}{R_o}\right)\right], \tag{33}$$

where $R_{av_i} = R_i + h'/2$, $R_{av_o} = R_o - h'/2$, α_{av_i} is the fractional area change of the midsurface of the inner layer and α_{av_o} is the fractional area change of the midsurface of the outer layer. Recognizing that $\sigma_{r_o} = -P_m$ at $r = R_o - h'$ and $\sigma_{r_i} = -P_m$ at $r = R_i + h'$, we can combine Eqs. 32 and 33 to eliminate P_m and obtain the radial force balance for the double shell:

$$P_i - P_o = K\frac{\alpha_{av_i} + 1}{R_{av_i}}h' + \frac{\alpha_{av_o} + 1}{R_{av_o}} - \ln\frac{(R_i + h')R_o}{(R_o - h')R_i}, \tag{34}$$

where we have let the moduli of the two layers be equal: $K_i = K_o = K$. This result can be simplified by using a series approximation for the logarithmic terms (Eq. 18) and neglecting terms of order $(h'/R_{av})^4$:

$$P_i - P_0 \simeq \frac{2Kh'}{R_{av}}\left[\alpha_{av} - \Delta\alpha_{av}\left(\frac{h_m + h'}{2R_{av}}\right)\right] - \frac{Kh'^3}{12R_{av}^3}. \tag{35}$$

Here we have substituted $\alpha_{av} = (\alpha_{av_i} + \alpha_{av_o})/2$ and $\Delta\alpha_{av_o} = (\alpha_{av_o} - \alpha_{av_i})/2$. Thus we see that for the bilayer there are three main contributions from the membrane to balance the transmembrane pressure difference. The first term corresponds to the membrane stress resultant, the second

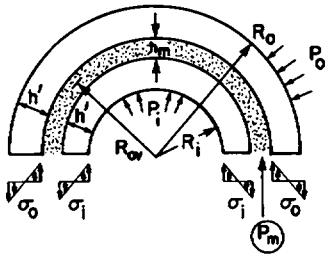

FIGURE 7 Cross-sectional view showing the radial force-balance for a double thick shell. The inner and outer pressures are P_i and P_o and the pressure at the center of the membrane is P_m. The thickness of each layer is h', and the distance between the layers is h_m. The inner radius is R_i, the outer radius is R_o and the radius of the membrane center is $R_{av} = (R_i + R_o)/2$. The surface-isotropic stresses in the inner (σ_i) and the outer (σ_o) layers are radially dependent.

term is a bending resistance resulting from the difference in the stress resultants in the inner and outer layers, and the last term represents the intrinsic bending resistance of each individual monolayer. Also note that as the radius of curvature becomes large compared with the membrane thickness, we recover the thin membrane result. Letting $K_m = 2Kh'$ we find:

$$P_i - P_o = \frac{K_m \alpha_{av}}{R_{av}}, \qquad \frac{h}{R_{av}} \to 0. \tag{36}$$

Axial Force Balance

The sum of forces in the axial direction is (see Fig. 8)

$$\int_{R_i}^{R_i+h'} \bar{\sigma}_i r dr + \int_{R_o-h'}^{R_o} \bar{\sigma}_o r \, dr = P_m R_{av} h_m + \frac{P_i}{2} R_i^2 - \frac{P_o}{2} R_o^2 + \frac{f}{2\pi}. \tag{37}$$

The integrals in Eq. 37 are evaluated using Eq. 14 applied to each layer and Eqs. 32 and 33 for the radial stresses in each shell. Taking the elastic moduli of the two layers to be equal we find

$$\frac{Kh'}{2}(\alpha_{av_i} + 1) R_{av_i}\left[1 + \frac{h'^2}{12R_{av_i}^2}\right] + (\alpha_{av_o} + 1) R_{av_o}\left[1 + \frac{h'^2}{12R_{av_o}^2}\right] - Kh'R_{av} = \frac{f}{2\pi}. \tag{38}$$

This result can be simplified using a series expansion to express $1/R_{av_i}^2$ and $1/R_{av_o}^2$ in terms of R_{av}^2 and power series in h/R_{av}:

$$\frac{1}{R_{av_o}^2} = \frac{1}{R_{av}^2}\left[1 - \frac{h_m + h'}{R_{av}} + 3\left(\frac{h_m + h'}{2R_{av}}\right)^2 - 4\left(\frac{h_m + h'}{2R_{av}}\right)^3 + \cdots\right]$$

and

$$\frac{1}{R_{av_i}^2} = \frac{1}{R_{av}^2}\left[1 + \frac{h_m + h'}{R_{av}} + 3\left(\frac{h_m + h'}{2R_{av}}\right)^2 + 4\left(\frac{h_m + h'}{2R_{av}}\right)^3 + \cdots\right]. \tag{39}$$

Using these expansions and neglecting terms of order $[(hm + h')/2\,R_{av}]^2$, Eq. 37 becomes

$$\frac{f}{2\pi} \simeq Kh'R_{av}\left[\alpha_{av} + \Delta\alpha_{av}\left(\frac{h_m + h'}{2R_{av}}\right)\right] + \frac{Kh'^3}{12R_{av}}. \tag{40}$$

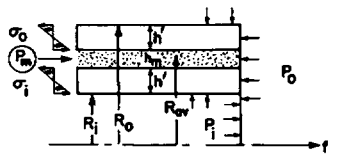

FIGURE 8 Cross-sectional view of the upper half of the cylinder showing the axial force balance. In addition to the quantities defined in Fig. 7, the axial force f is shown.

Again there are three main components to the membrane response to the applied force: the stress resultant, a bending resistance due to the difference between the stress resultants in the inner and outer layers, and the intrinsic bending resistance of the individual layers. Eqs. 35 and 40 can be combined to obtain a relationship between the external forces and the dimensions and properties of the tether. Recognizing that $(P_i - P_o)/R_{av}^2 \ll f/2\pi$, we find

$$\frac{f}{2\pi} \simeq Kh'\Delta\alpha_{av}(h_m + h') + \frac{Kh'}{6}\frac{h'^2}{R_{av}}. \tag{41}$$

Slip

In Eq. 41 the second term on the right accounts for the bending of each liquid shell while the first depends on the difference in the average expansion (or compression) between the two shells. If the monolayers are unconstrained and can slide freely relative to each other, the average stress in each layer will be the same, and $\Delta\alpha_{av} = 0$. If we let $h_m = 0$ (see Figs. 7 and 8), then $h' = h/2$ and Eq. 41 becomes

$$\frac{K_m h^2}{48}\frac{1}{R_{av}} = \frac{f}{2\pi}. \tag{42}$$

Eq. 42 when compared with Eq. 24 shows that if a single liquid shell subjected to a force f was cut down the middle and each half was unconstrained and allowed to slide freely, then the average radius of the cut shell would decrease to one-fourth of its original value.

At the opposite extreme from "free slip" is the case where the two layers of a double-shelled tether are tightly coupled together. This could be accomplished by capping the ends of the tether or "gluing" the two surfaces together. For this case, let $h_m = 0$ and note that

$$\Delta\alpha_{av} = \frac{\alpha_{av_o} - \alpha_{av_i}}{2} \simeq \frac{R_{av_o} - R_{av_i}}{2R_{av}} = \frac{h'}{2R_{av}}. \tag{43}$$

The substitution of Eq. 43 into Eq. 41 gives

$$\frac{K_m h'^2}{12R_{av}} + \frac{K_m h'^2}{4R_{av}} = \frac{K_m h^2}{12R_{av}} = \frac{f}{2\pi}, \tag{44}$$

which is, as expected, the result for a single liquid shell (Eq. 24).

Because of the lamellar molecular structure of a real membrane, the constituent monolayers can slip relative to each other. However, because the red cell or vesicle is a closed capsule, the amount of slip that can occur is limited. To evaluate the "slip term" in Eq. 41 for a tether formed from a closed surface, imagine the system to consist of a spherical cell body, the tether and a membrane projection into a pipette (Fig. 1 *b*). Again for simplicity, let $h_m = 0$. For this case, the area of the cell A_c is

$$A_c = 2\pi R_p L_p + 4\pi R_c^2 - \pi R_p^2 + 2\pi R_{av} L_t, \tag{45}$$

where R_c is the radius of the cell, R_p is the radius of the pipette, L_t is the length of the tether, and L_p is the length of the projection into the pipette. Expressions for the outer or inner areas of the monolayers are obtained by adding or subtracting $h'/2$ from R_p, R_c, and R_t in Eq. 45. Because an increase in the length of the tether requires displacement of material from the pipette, a relationship exists between the tether radius R_t, its length L_t, the pipette radius R_p, and the change in the length of the projection in the pipette as the tether is formed ΔL_p: $R_t L_t \simeq -R_p \Delta L_p$ (Hochmuth and Evans, 1982). Using this expression and the expressions for the areas of the inner and outer monolayers, we can estimate $\Delta\alpha_{av}$:

$$\Delta\alpha_{av} \simeq \frac{A_o - A_i}{2A_{av}} = \frac{h'(L_t + L_{po} + 4R_c - R_p)}{A_c/\pi}, \quad (46)$$

where L_{po} is the length of the projection in the pipette when $L_t = 0$.

When Eq. 46 is substituted into Eq. 41, an expression for the "slip" term in terms of the tether length is obtained. For a given tether force f, the tether length will have a significant influence on the tether radius when the second term in Eq. 41 becomes comparable to the first. These terms are equal when

$$L_t = \frac{A_c}{6\pi R_t} - L_{po} - (4R_c - R_p). \quad (47)$$

When $R_c = 3.06$ μm, $R_p = 1.0$ μm, and $L_{po} = 4.0$ μm, the calculated value for A_c is 140 μm^2. With $R_t = 20$ nm, the calculated value for L_t from Eq. 47 is 360 μm. Thus, a tether must reach a length in excess of 300 μm before the "slip" term is comparable to the bending term in Eq. 41. Usually experiments are performed with tethers <100-μm long, and the slip term can be neglected.

DISCUSSION

In analyses of the deformations of biological membranes, the membrane is usually treated as a very thin material and the state of stress in the plane of the membrane is defined in terms of stress resultants, which are integrals of the stresses over the thickness of the membrane. This is a very successful technique as long as the thickness of the membrane is small compared with the principal radii of curvature. However, membrane tethers can have radii as small as 10 nm, only four times larger than the thickness of a phospholipid monolayer. In this case, the membrane cannot be considered "thin." To analyze the deformation of a tether we postulate a three-dimensional state of stress in which the stress is isotropic in the plane of the membrane (i.e., $\sigma_\phi = \sigma_z$). This model preserves the "two-dimensional liquid" character of the membrane and allows the liquid tether to achieve static equilibrium when exposed to an axial load even though the stress resultants are anisotropic.

As long as the tether is short enough to permit the slip term in Eq. 41 to be neglected, our analysis predicts the experimental observation that the axial force and the tether radius are inversely related to each other. This force–radius relation can be written in terms of a bending constant B':

$$\frac{B'}{R_{av}} = \frac{f}{2\pi}. \quad (48)$$

where

$$B' = K_m h'^2/12. \quad (49)$$

The thickness of a monolayer is h' and K_m is equivalent to the area expansion modulus for a bilayer membrane. The coefficient B' is thermodynamically equivalent to the bending stiffness defined by Evans and Skalak (1979). A value for the bending constant B' (and thus a value for the area modulus K_m) can be calculated using Eq. 36 and the experimental data of Hochmuth et al. (1982) for normal, human red cell membrane. In these experiments, the tether force f was not measured directly, but it can be deduced from measured values of the isotropic tension in the cell membrane, T. If we assume that the isotropic tension in the membrane is continuous and becomes equal to the axial stress resultant in the tether T_z, and if we assume that $2\pi R_{av} T_z = f$ (Hochmuth and Evans, 1982; Waugh, 1982*a*), then

$$B' = R_{av}^2 T. \quad (50)$$

Recently, Gilbert and Hochmuth (unpublished observa-

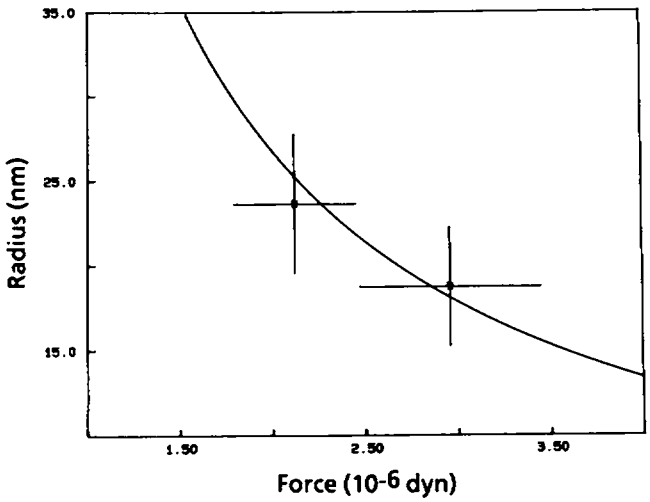

FIGURE 9 Force dependence of tether radius. Data were obtained from Gilbert and Hochmuth (unpublished observations). The force was calculated from measurements of membrane tension ($f = 2\pi R_{av} T$). A total of seven cells were measured. In five cases a consistent dependence of tether radius on force was observed. Two cells showed negligible dependence of radius on force. Average values for the five cells that exhibited a force-dependent tether radius are indicated by the stars in the figure. Error bars represent plus or minus one standard deviation ($n = 5$). The solid line gives the theoretical prediction (Eq. 48) for a bending stiffness, $B' = 0.85 \times 10^{-12}$ dyn cm.

tions) repeated the experiments of Hochmuth et al. (1982) for normal, human red cell membrane. They found that for a given T, the value for R_{av} was ~15% greater than that previously reported. Their data are shown in Fig. 9 along with the theoretical prediction based on Eq. 48, and a value for B' of

$$B' = 0.85 \times 10^{-12} \text{ dyn cm.}$$

For $h' = 2.0$ nm, the value for K_m calculated via Eq. 49 is

$$K_m = 250 \text{ dyn/cm.}$$

These values are consistent with values for the membrane properties measured with other techniques. Evans (1983) obtained a value of 1.8×10^{-12} dyn cm for the bending modulus of the erythrocyte membrane from observations of surface buckling as cells were aspirated into micropipettes. Those measurements probably include contributions from both the membrane bilayer and the membrane skeleton. Thus, our value of 0.8×10^{-12} dyn cm for tethers (which probably comprise only bilayer) represents a reasonable fraction of Evans' value. A value of 450 dyn/cm for the area expansivity modulus of red cell membrane was measured by Evans and Waugh (1977) by micropipette aspiration. Kwok and Evans (1981) measured the expansivity modulus for egg lecithin bilayers and obtained a value of 125 dyn/cm. Recently, Evans and Needham (1986) found that addition of cholesterol to bilayers increases the modulus severalfold, but that the increase is mitigated by the further addition of protein into the surface. Thus, our value of 250 dyn/cm falls within the range reported for bilayers and is smaller than the red cell membrane expansivity by about a factor of two. The present analysis yields reasonable values for material properties and provides a theoretical framework for interpretation and design of future experiments. Application of this analysis to precise measurements of the force-dependence of tether radius will provide a novel, independent method for determining bilayer expansivity and bending stiffness.

The assumption of incompressibility is based on a comparison of the volumetric compressibility and area compressibility moduli of bilayers. Srinivason et al. (1974) applied volume dilatometry to hydrated amphiphilic bilayers. Based on their measurements, a value of 10^{10}–10^{11} dyn/cm^2 has been estimated for the volumetric modulus (Evans and Hochmuth, 1978). The area compressibility modulus of bilayers depends on their composition, but falls in the range of 100–800 dyn/cm (Evans and Needham, 1986). Dividing by the membrane thickness (~50 nm) we estimate a three-dimensional area modulus of on the order of 10^9 dyn/cm^2, one to two orders of magnitude smaller than the volumetric modulus. Thus, the assumption of incompressibility is justified.

The assumption of surface-isotropy in the stresses ($\sigma_\phi = \sigma_z$) is based on observations of the mechanical behavior of large, thin-walled phospholipid vesicles above the phase transition. When aspirated into micropipettes, the vesicles deform freely until further deformation is limited by the fixed surface area and volume of the vesicle. To describe this behavior, Evans and Skalak (1979) and Waugh (1982*a*) used a constitutive model of a two-dimensional Newtonian-like fluid, for which the surface shear resultant is direcly proportional to the rate of surface shear deformation. Under static conditions, the surface shear resultant is identically zero. This model is consistent with the molecular organization of the bilayer. There are no molecular associations between adjacent molecules in the surface to elastically support significant surface shear resultants. In the present analysis we have extended earlier two-dimensional liquid models to three dimensions. We postulate that under static conditions, shear stresses in directions tangent to the surface plane are identically zero. The model is consistent both with the observation that bilayer membranes exhibit no surface shear elasticity and the lack of intermolecular associations along the entire length of the amphiphilic molecules that constitute the bilayer.

A limitation of the applicability of this theory may come from the linear constitutive relationship that is used (Eq. 7). For extremely small tethers ($R_{av} \simeq 8.0$ nm), maximum strains could approach 25%. For such large deformations, it is entirely possible that the linear relationship will not apply. Other constitutive relationships could be used in the present theoretical framework to account for nonlinearities in the stress–strain relationship. For example, a two-dimensional van der Waals equation of state could be used. A second limitation may result from the assumption that K is constant over the thickness of the monolayer. Clearly, the molecules of the surface are heterogeneous along their length. If there were significant variations in K along the length of the molecule, the predictions of the present analysis might be inaccurate. By allowing for the existence of a three-dimensionally isotropic liquid layer at the center of the membrane, we have tried to accommodate some variation in K within the present model. To account for variations in K along the length of the molecules more precisely, a detailed statistical analysis of the molecular interactions would be required. Such an analysis is beyond the scope of the present work. In the present analysis we have attempted to capture the essential features of the membrane mechanical behavior with a minimum of algebraic complexity. In the event that the present theoretical predictions are not born out by further experiments, more complex constitutive relationships could be incorporated into the analytical framework. At present, the need for such additional complexity has not been demonstrated.

Because the monolayer of a lipid bilayer comprises only 20 or so molecular units in the thickness direction, the application of continuum theory, in which there is defined a local state of stress that varies with position, might be questioned. In general, the internal stress arises from the forces between molecules in the material. These forces vary as the molecules are moved together or apart by deforming

the material. In classical continuum theory local molecular fluctuations are removed by averaging over space. This is impossible to do across the thickness of a biomembrane because it is so thin. Therefore, in the present analysis we postulate that the stress represents a time-averaged force per molecule. This removes the effect of molecular fluctuations at a point. Application of a continuum theory at the molecular level has been used successfully in the past. For example, the diffusivity of molecules is accurately predicted with the Stokes–Einstein equation. Justification for using a continuum theory at a molecular level rests on the accuracy and reliability of its predictions. That the present analysis yields values for membrane expansivity and bending stiffness that are consistent with other methods is important preliminary justification for this approach. However, additional experiments will be needed to test the reliability of our predictions.

APPENDIX

Thermodynamic Development of the Constitutive Equation

The constitutive equations for the shell must reflect the actual membrane behavior. The essential features of this behavior are low (zero) shear rigidity, small area expansivity, and volumetric incompressibility. Therefore, to describe the behavior of the membrane mathematically we first identify parameters that characterize these three different modes of deformation: volume change, area (or thickness) change, and surface shear. To characterize the change in volume we simply use the fractional volume change:

$$\nu \equiv \lambda_z\lambda_\phi\lambda_r - 1. \tag{A1}$$

To characterize the surface shear, we use the normalized extension ratio, $\tilde{\lambda}$, defined by Evans and Skalak (1979) for two-dimensional continua:

$$\tilde{\lambda} \equiv \sqrt{\lambda_z/\lambda_\phi}. \tag{A2}$$

The choice of an area deformation parameter is less obvious. Use of the fractional area change ($\alpha = \lambda_z\lambda_\phi - 1$) is inappropriate because the functions ν, $\tilde{\lambda}$, and α are not linearly independent. (The Jacobian J is zero when $\lambda_z = \lambda_\phi$.) That at constant volume an increase in material area requires a decrease in material thickness provides us with a clue to the proper form of the area parameter, namely, that it ought to contain the ratio of the area change ($\lambda_z\lambda_\phi$) to the thickness change (λ_r):

$$\tilde{\alpha} \equiv \sqrt{\lambda_z\lambda_\phi/\lambda_r} - 1. \tag{A3}$$

The square root is introduced so that $\tilde{\alpha}$ will reduce to α for the incompressible case. Note that for $\nu = 0$, $\lambda_r = 1/\lambda_z\lambda_\phi$ and

$$\tilde{\alpha} = \lambda_a\lambda_\phi - 1 = \alpha. \tag{A4}$$

The parameters ν, $\tilde{\lambda}$, and $\tilde{\alpha}$ are linearly independent ($J = \lambda_z/\sqrt{\lambda_r} \neq 0$ for all λ's). This is an essential characteristic for the thermodynamic treatment to follow because it must be possible to vary the different parameters independently. Next we identify the stress terms that are conjugate to the deformation parameters. To do this, consider the work done on a material element (Fig. 2) for a small variation in the deformed state. In terms of the principal stresses and the principal extension ratios, the variational work per unit undeformed volume (dW/V_o) for the differential element is

$$\frac{dW}{V_o} = \sigma_\phi\lambda_z\lambda_r\delta\lambda_\phi + \sigma_z\lambda_\phi\lambda_r\delta\lambda_z + \sigma_r\lambda_\phi\lambda_z\delta\lambda_r, \tag{A5}$$

where δ indicates a virtual change in the extension ratio. With Eqs. A1–A3, Eq. A5 can be re-expressed in terms of the parameters, ν, $\tilde{\alpha}$, and $\tilde{\lambda}$:

$$\frac{dW}{V_o} = \frac{\sigma_r + \bar{\sigma}}{2}d\nu + (\bar{\sigma} - \sigma_r)\frac{(\nu + 1)}{(\tilde{\alpha} + 1)}d\tilde{\alpha} + 2\sigma_s(\nu + 1)\frac{d\tilde{\lambda}}{\tilde{\lambda}}, \tag{A6}$$

where $\bar{\sigma} = (\sigma_z + \sigma_\phi)/2$ and $\sigma_s = (\sigma_z - \sigma_\phi)/2$. Eq. A6 appears complicated because of the scaling terms $\nu + 1$ and $\tilde{\alpha} + 1$. Recognizing that for an incompressible membrane with small area expansivity these terms are approximately unity, we are left with just the sum of the products of each deformation parameter and its conjugate stress. Each parameter is functionally related to its conjugate stress. This conclusion is based on a thermodynamic argument: For a system with three independent reversible work modes (given by ν, $\tilde{\lambda}$, and $\tilde{\alpha}$) there are four degrees of freedom. For an isothermal deformation, the work on the system is equal to the change in the Helmholtz free energy. Thus, an isothermal deformation can be considered to be a change in the state of the system, specified by ν, $\tilde{\lambda}$, and $\tilde{\alpha}$. Because the parameters are linearly independent we can hold any two fixed and vary the third. Fixing of two parameters and the condition that the deformation be isothermal places three constraints on the system, leaving one degree of freedom for variations in the third parameter. Because there is only one degree of freedom, the parameter and its coefficient (conjugate stress) cannot be varied independently, i.e., they must be functionally related. These functional relationships represent isothermal equations of state (see Evans and Skalak, 1979). Thus, we expect there to be a relationship between ν and the sum $\bar{\sigma} + \sigma_r$, between $\tilde{\alpha}$ and the difference $\bar{\sigma} - \sigma_r$, and between $\tilde{\lambda}$ and the quantity σ_s. The form of these equations depends on the nature of the material. For bilayer membranes, two of these equations are trivial. The incompressibility condition requires that $\nu = 0$. The lack of shear rigidity requires $\sigma_s = 0$. Because the changes in surface area are small, the third relationship can be expressed as a simple linear relationship:

$$\bar{\sigma} - \sigma_r = K\tilde{\alpha}. \tag{A7}$$

For the case of an incompressible membrane, $\tilde{\alpha} = \alpha$, and the constitutive relationship given in Eq. 7 is obtained.

The reader should be advised that we have neglected transverse shear throughout this discussion. This is appropriate in the present circumstances because of the symmetry of the cylindrical geometry and the loading conditions. In general, however, the transverse shear may not be negligible, and the present development may need to be expanded to include it.

This work was supported by National Institutes of Health grants HL-23728 and HL-27502 (to R. M. Hochmuth) and HL-18208 and HL-31524 (to R. E. Waugh).

Received for publication 19 June 1986 and in final form 1 May 1987.

REFERENCES

Berk, D. A., and R. M. Hochmuth. 1986. Diffusion in erythrocyte membrane tethers. *Biophys. J.* 49 (2, Pt. 2): 312a. (Abstr.)

Evans, E. A. 1983. Bending elastic modulus of red blood cell membrane derived from buckling instability in micropipette aspiration tests. *Biophys. J.* 43:27–30.

Evans, E. A., and R. M. Hochmuth. 1978. Mechanochemical properties of membranes. *Curr. Top. Membr. Transp.* 10:1–64.

Evans, E., and D. Needham. 1986. Giant vesicle bilayers composed of mixtures of lipids, cholesterol and polypeptides: thermomechanical and (mutual) adherence properties. *Faraday Dis. Chem. Soc.* 81:267–280.

Evans, E. A., and R. Skalak. 1979. Mechanics and thermodynamics of biomembranes. *CRC Crit. Rev. Bioeng.* 3:181–418.

Evans, E. A., and R. Waugh. 1977. Osmotic correction to elastic area compressibility measurements on red cell membrane. *Biophys. J.* 20:307–313.

Hochmuth, R. M., and E. A. Evans. 1982. Extensional flow of erythrocyte membrane from cell body to elastic tether: I. Analysis. *Biophys. J.* 39:71–81.

Hochmuth, R. M., E. A. Evans, and D. F. Colvard. 1976. Viscosity of human red cell membrane in plastic flow. *Microvasc. Res.* 11:155–159.

Hochmuth, R. M., N. Mohandas, and P. L. Blackshear, Jr. 1973. Measurement of the elastic modulus for red cell membrane using a fluid mechanical technique. *Biophys. J.* 13:747–762.

Hochmuth, R. M., H. C. Wiles, E. A. Evans, and J. T. McCown. 1982. Extensional flow of erythrocyte membrane from cell body to elastic tether: II. Experiment. *Biophys. J.* 39:83–89.

Koppel, D. E., M. P. Sheetz, and M. Schindler. 1981. Matrix control of protein diffusion in biological membranes. *Proc. Natl. Acad. Sci. USA.* 78:3576–3580.

Kwok, R., and E. Evans. 1981. Thermoelasticity of large lecithin bilayer vesicles. *Biophys. J.* 35:637–652.

Skalak, R., A. Tozeren, R. P. Zarda, and S. Chien. 1973. Strain energy function of red blood cell membranes. *Biophys. J.* 13:245–264.

Srinivason, K. R., R. L. Kay, and J. F. Nagle. 1974. The pressure dependence of the lipid bilayer phase transition. *Biochemistry.* 13:3494–3496.

Waugh, R. E. 1982*a*. Surface viscosity measurements from large bilayer vesicle tether formation: I. Analysis. *Biophys. J.* 38:19–27.

Waugh, R. E. 1982*b*. Surface viscosity measurements from large bilayer vesicle tether formation: II. Experiments. *Biophys. J.* 38:29–37.